# CORRELATIONS BETWEEN DYNAMIC THERMAL PROPERTIES, ENERGY CONSUMPTION AND COMFORT IN WOOD, CONCRETE AND LIGHTWEIGHT BUILDINGS

Alexandre Pépin, Louis Gosselin*, Jonathan Dallaire

Department of Mechanical Engineering, Université Laval, Québec City, QC, Canada, G1V 0A6

**Article accepté pour publication dans :** Transactions of the Canadian Society for Mechanical Engineering, Volume 45, 25 February 2020.

* Corresponding Author: Louis.Gosselin@gmc.ulaval.ca; Tel.: +1-418-656-7829; Fax: +1-418-656-5343.

**Abstract**

An office building located in Quebec City (Canada) with different envelope assemblies has been simulated in order to determine the energy consumption and thermal comfort that they provide. The resistance, thermal mass, and materials (concrete, cross-laminated timbers (CLT), and light-frame) are varied in a series of 164 different scenarios and the energy intensities for heating and cooling determined in each case, along with the discomfort index. Results show that the materiel used to provide thermal mass has a larger impact on comfort and energy consumption than the value of the thermal mass thickness itself. It was also attempted to correlate the performance of the envelope assessed through energy simulations with four dynamic thermal properties (i.e., dynamic transmittance, areal heat capacity, decrement factor, and time lag). The internal areal heat capacity appeared to be the most important variable to explain variations of performance of the envelope.

*Keywords*: thermal mass; wood; concrete; dynamic thermal properties; office building; comfort; energy savings

**Nomenclature**

| | |
|---|---|
| $c_p$ | specific heat [J/kg-K] |
| $COP$ | coefficient of performance [-] |
| $DDH$ | degree discomfort hour [°C-h] |
| $DDH^+$ | discomfort index when the temperature is too high [°C-h] |
| $DDH^-$ | discomfort index when the temperature is too low [°C-h] |
| $e$ | transfer matrix of a layer |
| $E$ | transfer matrix of the wall assembly |
| $f$ | decrement factor [-] |
| $k$ | thermal conductivity [W/m-K] |
| $l$ | layer thickness [m] |
| $L$ | thermal mass thickness [m] |
| $n$ | total number of layers in the wall assembly |
| $P$ | period [s] |
| $R''$ | thermal resistance [$m^2$-K/W] |
| $T$ | temperature [°C] |
| $U$ | static transmittance [W/$m^2$-K] |
| $\lvert Y_{12} \rvert$ | dynamic transmittance [W/$m^2$-K] |

*Greek symbols*

| | |
|---|---|
| $\kappa_1$ | internal areal heat capacity [kJ/$m^2$-K] |
| $\Delta t$ | time interval [h] |
| $\rho$ | density [kg/$m^3$] |
| $\phi$ | polar angle [-] |
| $\tau$ | time lag [h] |

*Subscripts*

| | |
|---|---|
| $csp$ | cooling setpoint |
| $hsp$ | heating setpoint |
| $i$ | occupancy hour index |

| | |
|---|---|
| *j* | property of the $j^{th}$ layer of the wall assembly |
| *op* | operative |

## 1. Introduction

In the design of a building envelope, occupants' comfort and energy consumption are two important aspects to consider. In addition to the thermal resistance of the envelope, the value of which is often provided by regulations or standards, its thermal mass also has a role to play regarding energy consumption and comfort (Ascione et al., 2015; Sadineni et al., 2011). Recognizing thermal mass impact on building performance, Wang et al. (Wang et al., 2014) proposed thermal mass requirements to complement US building codes. Concrete is often considered to provide a high thermal mass in buildings. However, concrete has a significant carbon footprint, which can result in a challenge when aiming at sustainability (Cole, 1999). For example, Hacker et al. (Hacker et al., 2008) investigated the trade-offs between providing more thermal mass (concrete) to reduce energy consumption and operational $CO_2$ emissions versus the embodied $CO_2$ of concrete. Phase change materials have also been investigated in order to increase the thermal mass of envelope assemblies (Arnault et al., 2010; Chwieduk, 2016), but cost, fire prevention regulations and environmental impacts of these materials (often derived from petroleum) limit their utilization. Therefore, a lot of attention has been devoted lately to wood and bio-based materials as greener and more sustainable material alternatives (Lo, 2017; Ramage et al., 2017). Studies have shown that the use of wood in buildings can help reducing the carbon emissions related to building materials (Ximenes and Grant, 2013). On the other hand, wood has a higher conductivity than typical insulation materials, but a lower thermal mass than concrete (Czajkowski et al., 2016), which might lead designers to consider it as being detrimental to building energy performance. It is not always clear how the heating/cooling needs and comfort could be affected by this material. In particular, there are still a lot of challenges to fully understand the thermal mass of wood in different contexts.

Recent studies on thermal mass and dynamic behavior of envelopes often conclude that with high thermal mass envelopes, building peak loads are diminished and so is the

energy consumption (Aste et al., 2009; Kossecka and Kosny, 2002). Moreover, the best envelope composition is usually obtained by placing the insulation close to the external surface and the thermal mass, close to the interior (Di Perna et al., 2011; Gregory et al., 2008). On the other hand, thick insulation can cause summer overheating when coupled with high thermal mass (Stazi et al., 2013).

Al-Sanea et al. (Al-Sanea et al., 2012) have numerically investigated the effects of thermal mass with a 1D finite difference approach on variables such as the transmission loads, energy storage rate, time lag, and decrement factor in the climate of Riyadh, Saudi Arabia. Heavyweight concrete was the material providing the thermal mass in the wall composition, and therefore, the thickness of the concrete layer was varied in the study to change the wall thermal mass. They found that the heating and cooling loads during winter and summer are not significantly changed by thermal mass. On the other hand, in the mid-seasons, the loads are greatly affected by thermal mass. They explain this situation by the fact that in the mid-season the building can be naturally ventilated and it can discharge at night the heat accumulated in the walls during daytime. Overall, transmission through the envelope was reduced by 17% for cooling and by 35% for heating as a result of optimizing the thermal mass in this study. Zhu et al. (Zhu et al., 2009) studied a high thermal mass insulated concrete wall system for a zero energy house in Las Vegas, Nevada, USA and observed more stable temperature, reduced heating loads but increased cooling demands compared to lighter a wall construction.

The effect of thermal mass (concrete layer) on energy demand and comfort in Alaskan houses was simulated by Stevens et al. (Stevens et al., 2016). Due to the cold climate (heating degree days above 7000°C-day), thermal mass was not able to reduce heating loads. However, it yielded more comfortable conditions in the summer. With a conceptual model, Karlsson et al. (Karlsson et al., 2013) showed that although thermal mass affected the power consumption pattern under a cold climate, the total energy consumption was not always reduced. Aste et al. (Aste et al., 2009) have also investigated the effects of thermal mass of the envelope on the energy performance of buildings. They analyzed a series of envelopes and then performed energy simulations for a simple test cell. Their simulations were made for Milan, Italy. Parametric studies were performed by varying different building design features to understand when thermal mass was more

beneficial: with or without shading devices, low or high ventilation rate, one or four high thermal mass walls, intermittent or continuously operating HVAC systems, etc. Results show that the energy demands for heating and cooling could be reduced respectively by 10% and 20% as a result of using a high thermal mass envelope over a low thermal mass. Furthermore, their study highlights the fact that thermal inertia becomes more important when the inertia is coupled with other energy saving measures or strategies in the building, such as night ventilation (Ramponi et al., 2014; Yang and Li, 2008).

Based on measurements in Spanish schools and on simulations, Orosa and Oliveira (Orosa and Oliveira, 2012) demonstrated the impact of thermal mass on the energy performance. They explained that internal gains, solar heat gains, air-change rate, among others, can influence the role played by thermal mass, and argue that wall transmittance is not enough to fully characterize an envelope. Wooden panels used as permeable internal coverings were simulated and were found to increase the time constant of the building while reducing energy consumption.

The internal surface heat capacity is also important because its value characterizes the amount of heat that can be stored in the wall. Di Perna et al. (Di Perna et al., 2011) proposed threshold values for the internal areal capacity as a function of the transmittance value of the wall. Moreover, their results (which were obtained for a school in Loreto, Italy) demonstrated that no matter which window opening strategy was used, the comfort was always better in the building with a high thermal mass.

The above literature review revealed different limitations and challenges: Studies on thermal mass performed under colder climates such as that of Québec City, Canada (5202°C-days of heating) are scarce. Furthermore, investigations on the thermal mass provided by wood in the wall composition (e.g., with massive wood such as cross-laminated timber (CLT)) are also few. Finally, since the benefits of thermal mass depend on the context and overall building design, it can be challenging to assess the actual energy savings and comfort improvement related to the envelope. The main objective of the present paper is to offer some answers to these issues. Section 2 presents the details of the building energy model that was developed in Energy Plus. Three types of envelopes were simulated (concrete, CLT and light-frame). The impact of thermal resistance and thermal mass on energy intensity and comfort is detailed in Section 3. Section 4 presents how the

four dynamic properties of the envelopes considered in this study were calculated. The advantage of dynamic thermal properties is that they are easy and fast to calculate or to specify. Potential correlations between the resulting dynamic properties and energy intensity and comfort were explored in Section 5.

## 2. Transient energy and comfort modeling of the building

The building under study is an office building located in Quebec City (Quebec, Canada). In order to simplify the model, only an intermediate storey was considered. The dimensions of the floor are 23 m × 21 m. In order to simulate an intermediate floor, the ceiling and floor are considered adiabatic.

Three types of construction assembly for the walls have been considered. They are listed in Table 1. However, the floor construction, described in Table 2, stays the same for all simulations in this study to highlight the influence of the thermal mass of the envelope itself. The first type of envelope is made of cross-laminated timbers (CLT). CLT panels are massive components made of successive crosswise layers of lumbers aligned and glued together. The second type of construction is made of concrete. Finally, a third wall assembly was considered, i.e., light-frame. The properties of the different materials constituting the wall assemblies are given in Table 3 (*CIBSE Guide A: Environmental design*, 2006).

For the two heavyweight walls, the thermal mass thickness is varied from 0.0254 m to 0.508 m in the simulations. For all the walls, different insulation values have been simulated; from RSI 2 to RSI 10 (RSI stands for surface thermal resistance in $m^2K/W$). The thickness of insulation was adapted when the massive layer changed, so that the overall insulation level was kept constant. This allowed isolating the impact of thermal mass on building performance. For the lightweight wall assembly, only the R-value can be changed since there was no thermal mass layer in that assembly. Fig. 1 presents the simulation plan, i.e., the different scenarios simulated in this study. Note that for some cases, the simulations could not be performed when the RSI value without the insulation was already larger than the specified RSI value of the assembly.

The building model was initially built in Simergy, a graphical interface to Energy Plus. Building conditions and schedules were inspired from the ASHRAE 90.1-2007

standard (American National Standards Institute et al., 2007) as these were found to be representative modern buildings considered in this study. Thereafter, modifications to the model that could not be made directly in the interface have been made in EnergyPlus or with Eppy, a Python module. For example, the roof and the floor were considered adiabatic which was set up directly in Energy Plus. Other modifications to the model made in Energy Plus include the automatic parametric sweep over the thickness of the different envelope components and the choice of output parameters.

Typical characteristics of an office building were considered for the analysis:

- 20 $m^2$/person and the occupants are present following the occupation schedule of Table 4;
- 19.5 W/$m^2$ for lighting and plug loads;
- 31 W/person for hot water equipment;
- One thermal zone for the entire floor;
- Window-to-wall ratio of 30%;
- Heating set point of 22°C from 7:00 to 20:00 and 18°C during the night for the weekdays. For Saturdays, Sundays and holidays a set point of 18°C is used;
- Cooling set point of 24°C from 6:00 to 20:00 and 35°C during the night for the weekdays. For Saturdays, Sundays and holidays a set point of 35°C is used;
- An ideal load model was used to simulate the HVAC systems;
- No humidity control has been implemented.

Based on the result of the energy simulations, the energy requirement for heating and cooling has been computed for each scenario. The calculated values are the heating and cooling heat transfer rates that needed to be removed or added to the zone to maintain the setpoint. In order to obtain the energy consumption, the cooling load has been divided by the *COP* of the cooling equipment (assumed to be 3.22) and the heating load was kept as is, i.e., an efficiency of 100% was considered (e.g., electric heating, as typical in Quebec, Canada).

In order to assess the thermal comfort of the occupants, a discomfort index has been developed. The idea behind the criterion is similar to that of the degree-days. During each occupancy hour i, the operative temperature $T_{op,i}$ was compared to the cooling and heating setpoints, $T_{csp,i}$ and $T_{hsp,i}$. Whenever the operative temperature is within the range of the setpoints, the room was considered to be comfortable. Otherwise, the difference between the operative temperature and the setpoint, $DDH_i$, is calculated:

$$\begin{aligned} &if\ T_{op,i} > T_{csp,i} \quad \Rightarrow\ DDH_i^+ = \left| T_{op,i} - T_{csp,i} \right| \Delta t_i \\ &if\ T_{op,i} < T_{hsp,i} \quad \Rightarrow\ DDH_i^- = \left| T_{op,i} - T_{csp,i} \right| \Delta t_i \\ &\text{else} \qquad\qquad \Rightarrow DDH_i = 0 \end{aligned} \tag{1}$$

where $\Delta t_i = 1\text{h}$. In the end, the discomfort indices were obtained by summing the *DDH* values calculated at each hour:

$$\begin{aligned} DDH^+ &= \sum_{i=1}^{8760} DDH_i^+ \\ DDH^- &= \sum_{i=1}^{8760} DDH_i^- \\ DDH &= DDH^+ + DDH^- \end{aligned} \tag{2}$$

The value of $DDH^+$ and $DDH^-$ provides the level of thermal discomfort when the temperature is too high and too low respectively. Summing the two values provides an overall measure of discomfort over the year in the building. Therefore, the criteria in Eq. (2) allows comparing thermal comfort between different types of walls.

## 2.1. Model verification

In order to develop a better understanding of the Energy Plus model and of the Simeb assumptions, two cases were developed with the same building parameters, dimensions and materials. The ventilation rate has also been left at default values. Only the HVAC model was different between the two cases. In one case (which we developed entirely in Energy Plus), the "Ideal Loads" model is used and in the other one, DX Cooling Coil and Electric Heating Coil were simulated. For the DX cooling and electric coil case, the system was a Simeb archetype corresponding to a similar configuration (single zone ventilation). Simeb was developed to simulate buildings and evaluate the admissibility of

buildings to subsidies, based on either Energy Plus or DOE2. The program includes validated archetypes which are predetermined models to simulate typical buildings (Sansregret and Millette, 2009). Since an archetype is validated to produce typical building energy consumption results, it was decided to first compare our model with it.

Table 5 presents the results for the two cases. Again, the heating and cooling loads provided by the ideal loads have been translated in terms of energy consumption with a *COP* of 3.22 for cooling and an efficiency of 1 for the heating. Both these values of representative of systems typically found in Quebec, Canada. They do not change the energy simulation results, just the post-processing of these results.

Based on the comparison provided in Table 5, it was found that our model produces similar results compared to the archetype (11% difference for total energy intensity). The difference is slightly larger for the estimation of the cooling load which was found to be caused by the difference in the management of dehumidification between the two models. Nevertheless, the results of the proposed model are typical of what is expected for such a building.

Furthermore, the energy consumption results were compared to values available in literature. The average total consumption of commercial and institutional buildings in Canada including lighting, electric equipment and HVAC systems is 280 kW-h/m$^2$ ("ENQUÊTE SUR L'UTILISATION COMMERCIALE ET INSTITUTIONNELLE D'ÉNERGIE : BÂTIMENTS 2009 - M144-4-2-2013-fra.pdf," n.d.), with an estimated 53% of the total consumption used for heating and cooling ("Évolution de l'efficacité énergétique au Canada, de 1990 à 2009," n.d.). This leads to an energy consumption of ~148.4 kW-h/m$^2$ for cooling and heating only. The energy intensity obtained from the present model is of the same order of magnitude. Our value is slightly smaller, because the present model corresponds to a state-of-the-art modern building, whereas the Canadian average above corresponds to a value for the actual building stock, including many older and less efficient buildings.

In the end, the HVAC model "Ideal Loads" was thus used for its simplicity and generality (e.g., it is not dependant on specific features of pumps, fans, coils, etc.). In particular, since we are mostly interested in this paper by the difference of energy

consumption induced by changes to the envelope, this approach was deemed adequate for the purpose of the paper.

## 3. Energy consumption and comfort as a function of thermal mass and thermal resistance

As described above, a series of different envelope compositions have been defined and used to determine the energy consumption and thermal comfort in a reference building (Section 2). Three types of assemblies were studied, namely one in which thermal mass is provided by concrete, one with CLT (wood) and a light-frame wood structure (see Table 1 for more details). For the first two types of envelopes, different combinations of the RSI-value and of the thickness of the thermal mass layer (i.e., concrete or CLT) were simulated.

In Fig. 2, the heating, cooling, and total energy intensities are reported as a function of the RSI factor of the opaque envelope for the lightweight wall and three different thermal mass thicknesses for the concrete and wood walls (namely 0.0254 m, 0.254 m and 0.508 m). Obviously, in the case of the light frame wood structure, no thermal mass layer is present. It should be recalled that the energy intensity presented in this and subsequent figures only include the energy required for heating and cooling. The energy required for domestic hot water, plug loads, lighting, etc., was not included since it does not vary with the envelope. It can be seen in Fig. 2 that the thermal resistance of the walls has a strong impact on the energy consumption, with a diminishing return trend (i.e., at some point, adding more insulation provides only a marginal benefit). For the sake of comparison, ASHRAE 90.1-2010 demands an assembly with a minimal RSI ranging from ~2.5 $m^2$-K/W (massive walls) to ~3.5 $m^2$-K/W (wood frame) for the climate zone of Quebec City.

It can also be noted that for a given RSI-value, there is a difference in the energy intensity depending on which material is used in the wall composition. In Fig. 2, the concrete wall yields a smaller energy requirement, followed by the CLT and then the light frame. For a given RSI-value, variations in energy consumption due to materials are of the order of ~4% for this case. This variation is caused by the difference in the thermal mass properties (i.e., CLT vs concrete vs light-frame).

Since the climate considered is cold (5058 degree-days of heating, T99% = -23.3°C (American Society of Heating, Refrigerating and Air-Conditioning Engineers, 2013)) and

the building is heating dominated, insulation plays an important role for the energy efficiency of the building. It is expected that the higher the RSI-value, the lower the energy consumption. As can be seen in Fig. 2b, the total energy consumption decreases when the RSI-value increases. In the winter, internal heat gains help to compensate the heat loss through the envelope, and thus, large insulation level is beneficial. On the other hand, during the summer, a less insulated envelope (i.e., low RSI) could help to dissipate the heat gains through the envelope in some periods. Given that the summer days are not very hot in the location considered (T1% = 27.2°C (American Society of Heating, Refrigerating and Air-Conditioning Engineers, 2013)), this could allow to release heat, in particular during evenings and nights. Nevertheless, because the heating needs are more important than cooling needs for this building, higher RSI-values were found to be more beneficial.

In Fig. 3, the energy intensity is reported as a function of the thermal mass thickness for different values of the RSI. The color and symbol code is detailed in Table 6 and is used in subsequent figures. It is visible in Fig. 3 that for a given RSI value, slightly more energy is required with the CLT than with the concrete. Also, above a certain thickness of thermal mass, the energy consumption basically flattens and does not change any more even if more mass is added. For the cases tested, above ~0.1 m, adding more mass did not result in changes of the energy consumption.

The discomfort indices $DDH^{\pm}$ introduced in Section 2 are shown in Fig. 4a as a function of the thermal mass thickness for a fixed level of insulation. The total discomfort index *DDH* is shown in Fig. 4b. It should first be noted that the value of $DDH^{-}$ is much larger than $DDC^{+}$, which means that operative temperatures below the specified setpoint is more of an issue than larger operative temperatures in this building. Due to the fact that it is heating dominated, wall inner surface temperature might be lower than the setpoint in the winter, thus causing discomfort. For this case (RSI = 6), when more thermal mass is added, it first tends to increase the discomfort index, and then to decrease it. The same behavior is observed for both the concrete and CLT walls, even though the concrete wall provided a slightly more comfortable environment thermally speaking.

This can be explained by Fig. 5 which shows the internal surface temperature of the walls for three typical days of the year. The temperature values correspond to averages over the four façades of the building. During winter (Fig. 5a), adding more thermal mass

significantly reduced the daily swing of the wall surface temperature and keeps the surface temperature closer to its daily average value (i.e., ~19.5°C). The greatest gap between the setpoint and the surface temperature is observed from 11AM to 6PM, and the wall temperature is dropping when the thermal mass is increased, thus causing more discomfort. In the spring (Fig. 5b), the dynamic behavior of the wall surface temperature appears to be similar to the case of the winter. In the summer, the same behavior is also observed in Fig. 5c, i.e., a cooler surface when there is more mass. In this case, because the surface temperature becomes very high, a small thermal mass results in a poorer comfort in the zone during summer. There is thus a complex trade-off to be made in terms of summer and winter comforts. When more mass is included in the wall, comfort in the winter deteriorated while it increased in the summer. Since the reference building is dominated by heating, this explains why one sees the rise of the discomfort index as a function of the thermal mass in the left side of Fig. 4.

Figure 6 shows the mean daily surface temperature swing (i.e., daily difference between maximum and minimum surface temperature averaged over the year) as a function of the thermal mass thickness. Again, the meaning of the symbols is presented in Table 6. The temperature swing varied between 6°C and 8.5°C depending on the scenario considered. Again, above ~0.1 m of thermal mass, no visible reduction of the temperature swing is observed. One can observe that the overall resistance has only a weak effect on the temperature swing, whereas material does have a significant impact. It can be further noted that the temperature swing decrease explains why the discomfort index goes down as $L$ increases in Fig. 4. Indeed, a lower temperature swing means shorter periods when the surface temperature is outside the specified setpoints.

The insulation level also has an impact on the surface temperature and on thermal comfort, which can be seen by going back to Fig. 5. However, one can observe that the daily temperature variations do not change drastically with the RSI-value. The surface temperature tends to be slightly higher for walls with the highest RSI-value, which contributes to a higher operative temperature. This proves to be beneficial in the winter, but not necessarily in the summer.

As shown in this section, detailed simulations can provide an estimate of the energy and comfort performance of an envelope composition. On the other hand, it would be

attractive to be able to characterize the envelope performance by its dynamic properties without having to run energy simulations. The next sections explore this idea. The calculation procedure to obtain common dynamic properties is presented, followed by a comparison between them and the outcomes of the energy simulations.

## 4. Calculation of dynamic parameters of envelope

As explained above, an attempt was made to correlate the envelope energy performance with its dynamic thermal properties. This allows characterizing an envelope without having to perform an entire energy simulation. This section describes how the dynamic properties of the wall assemblies were determined, based on the procedure described in ISO 13786 (ISO 13786:2007, n.d.). The dynamic parameters provide a quick assessment of the transient thermal behavior of the envelope and are thus strongly affected by thermal mass. In practice, wall assemblies are often characterized only by their static transmittance, $U$ [W/m$^2$-K]. The U-value corresponds to the inverse of the RSI-value of the wall, i.e., the resistance assuming a steady-state temperature profile in the wall:

$$U = \frac{1}{\sum_{j=1}^{n} R''_j} \tag{3}$$

where the thermal resistance for heat transfer by conduction through the $j^{th}$ layer is given by:

$$R''_j = \frac{l_j}{k_j} \tag{4}$$

and $n$ is the total number of layers. Surface resistances for the boundary layers (including convection and radiation) are also considered on the external and internal walls of the assembly. In the present work, these resistances are equal to 0.06 and 0.12 m$^2$-K/W for the external and internal walls, respectively. $U$ is useful for the static analysis of a wall, but it is not suited to characterize its dynamic behavior. In particular, when the wall has a large thermal mass, it is unlikely that a steady-state profile will ever establish in the wall. Other indicators can be used to assess the heat transfer dynamics of a wall.

In this paper, a series of four dynamic heat transfer properties have been considered based on the assumption of a 24-hour periodic regime in the thermal mass: (i) dynamic transmittance, (ii) time lag, (iii) internal areal heat capacity, and (iv) decrement factor.

In order to calculate these properties, the procedure described in ISO 13786 (ISO 13786:2007, n.d.) was followed, where it is assumed that the temperatures and heat fluxes at the internal and external walls of the assembly vary sinusoidally over a period $P$ and can be represented by complex numbers with the phasor notation. Under this assumption, the complex amplitudes of temperature and heat flux on one side of the assembly can be related to the complex amplitudes of temperature and heat flux on the other side through the use of a heat transfer matrix $E$:

$$E = \begin{bmatrix} E_{11} & E_{12} \\ E_{21} & E_{22} \end{bmatrix} = e_n e_{n-1} \ldots e_3 e_2 e_1 \tag{4}$$

where the heat transfer matrix for the j$^{th}$ layer $e_j$ is a 2 by 2 transfer matrix with coefficients that depend on the layer's thermal properties (i.e., $k$, $\rho$, and $c_p$), its thickness $l_j$, the period $P$, the layer's surface resistance, etc.:

$$e_j = \begin{pmatrix} e_{11} & e_{12} \\ e_{21} & e_{22} \end{pmatrix} \tag{4}$$

In the end, the heat transfer matrix $E$ is obtained by multiplying the transfer matrix for all the individual layers of the assembly, see Eq. (4). Note that all coefficients of the matrix $E$ are complex numbers, see Ref. (ISO 13786:2007, n.d.) for more details. Based on the matrix *E*, the different dynamic parameters can be calculated.

First, the dynamic transmittance $Y_{12}$, which can be seen as the heat flow entering the zone due to a variation of the exterior-interior temperature difference, is obtained as follow:

$$Y_{12} = -\frac{1}{E_{12}} \tag{4}$$

In order to obtain a real scalar for the dynamic transmittance, one must compute the norm of the complex number, i.e., $|Y_{12}|$. The time lag (or time shift) $\tau$ of the dynamic

transmittance is related to the polar angle $\phi$ when the complex amplitude of $Y_{12}$ is written as a phasor, $|Y_{12}|e^{i\phi}$, as follow:

$$\tau = \frac{P}{2\pi}\phi \tag{4}$$

where $P$ is the period of the thermal solicitation. Here, $P$ = 86,400 s (24 h) was used which allows consideration of daily meteorological variations and temperature setbacks as described in (ISO 13786:2007, n.d.). Note that $\tau$ is an indication of the time lag between the external temperature variations and the internal heat flux through the envelope.

The third parameter of interest, the internal areal heat capacity, is obtained from the following expression:

$$\kappa_1 = \frac{P}{2\pi}\left|\frac{E_{11}-1}{E_{12}}\right| \tag{4}$$

It can be noted that the variable $\kappa_1$ is a measure of the capacity of the envelope to store heat coming from inside the building. An analogous property could be calculated (i.e., the external areal heat capacity), which would measure the capacity of the wall assembly to store heat coming from the outside. However, in our case, the thermal mass is located on the innermost part of the envelope (with respect to the insulation) and therefore $\kappa_1$ is more relevant.

Finally, the last dynamic parameter used in this study is the decrement factor, which is a measure of the attenuation of the thermal fluctuations through the envelope. It can be calculated as follow:

$$f = \frac{|Y_{12}|}{U} \tag{4}$$

A numerical code was developed in Matlab to calculate the four dynamic parameters described above. In order to validate the model, the results obtained by the code were compared to those presented in Chapter 15.3 of (Grenfell Davies, 2004) and to the "improved" external walls L02_k1, L03_k1, and L04_k1from Rossi and Rocco's work (Rossi and Rocco, 2014). The thermal properties for the different assemblies used to make the validation are shown in Table 7. As one can see in Tables 8 and 9, the results obtained with the program can be qualified as adequate with variations within ± 5% compared to the

dynamic properties calculated and presented in (Grenfell Davies, 2004; Rossi and Rocco, 2014). The result for which the difference is over 5 % is the time shift of the first wall. The reason is likely to be the film resistances since their values were not mentioned by Rossi and Rocco in their work. Since the first wall is not as thick as the others, the influence of the value of the film resistances is larger. For the L04_k1 wall, the difference in U-values is caused by rounding errors.

## 5. Dynamic properties versus energy intensity and comfort

The dynamic parameters introduced in Section 4 were calculated for each wall assembly for which an energy simulation had been run (i.e., 164 wall assemblies). The dynamic properties could then be compared to the results of the energy simulations presented in Section 3.

### 5.1. Impact of internal areal heat capacity

In Fig. 7, for the different scenarios considered, the internal areal heat capacity $\kappa_1$ is plotted against the mass thickness. The values range from 22.87 to 37.11 kJ/m$^2$-K. The concrete walls have the largest internal heat capacity, followed by the ones with CLT, and finally by the light-frame structures. As the thickness of the thermal mass increases, the internal areal heat capacity tends to flatten to a constant value that is independent of the RSI-value for a given material.

The total energy consumption as well as the ones for heating and cooling are plotted as a function of the internal areal heat capacity $\kappa_1$ in Fig. 8. Each point in the figure represents a different combination of thermal mass, resistance and materials that was simulated. For a given RSI value, it can be seen in Fig. 8a that both the heating and cooling needs tend to be reduced as $\kappa_1$ increases (~2% and 4% for heating and cooling, respectively). As a result, the total energy intensity (Fig. 8b) also tends to decrease with the areal internal heat capacity. In Fig. 8b, the impact of materials is obvious as points corresponding to different thermal mass materials are gathered together. When considering different materials, one can see that increasing the internal areal heat capacity of the wall generally leads to reducing the energy consumption.

A similar figure was built for the discomfort index as a function of the internal areal heat capacity, see Fig. 9. In Fig. 9a, increasing the internal areal heat capacity tends to increase slightly the time during which the operative temperature is too high, whereas the discomfort caused by too low operative temperatures is typically reduced when the internal areal heat capacity increases. The overall trend, Fig. 9b, is that the building is more comfortable when the internal areal heat capacity is larger. This follows the reasoning expressed previously in the end of Section 3.

Nevertheless, considering Fig. 8 and Fig. 9, it should be emphasized that the "trends" explained above are not perfect correlations. For example, one can see different levels of comfort or energy consumption for the same internal areal heat capacity. The general impact of the internal areal heat capacity seems to be significant when the type of thermal mass changes, but not as much when the mass thickness changes for a given material.

### 5.2. Impact of dynamic transmittance

In Fig. 10, the dynamic transmittance $|Y_{12}|$ of the different envelopes tested is reported as a function of the thermal mass thickness. It varies by several orders of magnitude, from ~$10^{-5}$ to ~$10^{-1}$ W/m$^2$-K. The dynamic transmittance tends to decrease when more thermal mass is added to the envelope, and when CLT is used over concrete.

In Fig. 11, the energy intensities are shown as a function of the dynamic transmittance. The heating demand (Fig. 11a) is mostly unaffected by $|Y_{12}|$ except at large $|Y_{12}|$ values (beyond ~0.02 W/m$^2$-K) where it tends to increase. A similar behavior is observed for the cooling demand, i.e., it is mostly unaffected by $|Y_{12}|$ except at high values. Overall, the total energy intensity in Fig. 11b thus presents curves that are essentially independent of $|Y_{12}|$ except when $|Y_{12}|$ reaches higher values.

Regarding the discomfort indices, one can see in Fig. 12a that variations of $DDH^+$ with respect to $|Y_{12}|$ are larger for concrete than for CLT, but stays relatively small. For $DDH^-$, Fig. 12a shows that no visible effect of $|Y_{12}|$ is visible, except again at higher $|Y_{12}|$

values (i.e., $|Y_{12}|$ > 0.02 W/m$^2$-K) for which the discomfort is reduced. The overall discomfort in Fig. 12b varies more with the material than with the value of $|Y_{12}|$.

### 5.3. Impact of decrement factor

From its definition, the decrement factor is related to the dynamic transmittance, see Eq. (10). Fig. 13 shows the decrement factor as a function of the dynamic transmittance for the different cases that were tested. The different straight lines on which points are aligned represent walls with different RSI-values and the slope of the lines is equal to the resistance. The decrement factor being linked to the dynamic transmittance only by a factor of proportionality, the main conclusions regarding these two dynamic properties are the same.

### 5.4. Impact of time lag

The last dynamic parameter is the time lag $\tau$, which represents the time between the external temperature variations and the fluctuations of the internal heat flux through the envelope, as was explained in Section 4. This parameter is depicted in Fig. 14 in the interval [-*P*, 0] as a function of the thermal mass thickness, for different R-values, and for different envelopes. It can first be observed that for a given envelope (concrete, CLT, or lightweight), increasing the thickness of the thermal mass results in a greater lag (in amplitude), with a maximum lag corresponding to the period *P* of the temperatures and heat fluxes fluctuations (i.e., -24 h). There is also an initial value for $\tau$ that is non-zero (even for the lightweight wall) and that is intrinsic to each envelope. This value depends on the overall wall composition (refer back to Table 1).

It is noteworthy to mention that due to the periodicity of the temperature and heat fluxes across the envelopes, $\tau$ also features a certain form of periodicity as a function of the thickness of the thermal mass, as can be seen in Fig. 14 for the CLT wall. For example, a lag of 24 h is actually equivalent to no lag (0 h) since a periodic profile over 24 h was assumed when developing the dynamic properties, see Section 4.

Figure 14 can be rationalized by considering the periodic penetration depth (defined as the depth at which the amplitude of the fluctuations are reduced by a factor "e") of the thermal mass layer, which depends on the thermal properties ($k$, $\rho$, and $c_p$), as well as on the

period *P*. In this case, the periodic penetration depths for the CLT and concrete walls are 0.0473 m and 0.1386 m, respectively (see (ISO 13786:2007, n.d.) for the relevant details on how to calculate the penetration depth). The fact that the CLT wall assembly has a much smaller penetration depth could explain why $\tau$ in Fig. 14 increases much faster for the CLT wall than for the concrete wall. Indeed, the periodic fluctuations within the CLT layer are much more dampened than in the concrete layer, thus increasing the lag. It is also important to mention that for very large values of *L*, $\tau$ is more or less meaningful since the amplitude of the temperature and heat fluxes variations at the internal wall are very small. This was demonstrated in Fig. 10, where the dynamic transmittances $|Y_{12}|$ of both envelopes decrease quickly as *L* increases. Note that the energy consumptions (heating, cooling, and total), as well as the discomfort indices ($DDH^{\pm}$ and *DDH*) were plotted against $\tau$, but no clear correlation was found and thus, these figures are not presented in the paper.

## Conclusions

In this paper, an energy simulation model was developed to compute the energy consumption for heating and cooling with different envelope combinations, for a building located in Quebec City, Canada. The model also determines the level of thermal comfort. A series of 164 envelope designs were tested, by varying the thermal mass thickness, materials, and insulation level. As expected, it was observed that the total energy consumption decreased with the insulating level. The choice of material and thickness of the thermal mass also influenced, to a lesser extent, the energy consumption. In particular, it appeared that there was no significant energy saving resulting from increasing the thermal mass thickness over 0.1 m. As for the discomfort, the material type was much more impactful than the thermal mass material thickness itself. The thickness of the thermal mass had a low impact on discomfort, especially for the $DDH^{-}$ index. For the $DDH^{+}$ index, the difference is more noticeable, but remains small.

Then, the potential of dynamic properties to predict the energy consumption and comfort have been examined. In most cases, it was hard to find clear correlations between the dynamic parameters and the energy consumption or the comfort in the present study (office building, cold climate). The dynamic parameter with the strongest correlations was found to be the internal areal heat capacity. These results are important in terms of energy

regulations and policy development: although thermal mass can have an impact on energy and comfort, it is not straightforward to specify thermal mass criteria. Benefits and drawbacks need to be cautiously examined in each case.

Future work could focus on different types of buildings or different locations, to verify if the conclusions of this paper still hold. Furthermore, it would be interesting to add in the model the possibility to simulate more advanced HVAC control that could take advantage of thermal mass to store or release heat/cold at appropriate times (e.g., predictive control) (Fadzli Haniff et al., 2013; Reynders et al., 2013; Rijksen et al., 2010). This could help solving the discomfort problems due to overheating in the summer, for example with night ventilation. Considering natural ventilation could also increase the benefits of the thermal mass. Finally, it would also be interesting to consider other types of thermal mass (e.g., phase change materials (Bastani et al., 2014)) and to study the impact of the internal thermal mass (e.g., floor slabs, partition walls).

**Acknowledgments**

This work was supported by the NSERC Chaire industrielle de recherche sur la construction écoresponsable en bois (CIRCERB).

## References


Al-Sanea, S.A., Zedan, M.F., Al-Hussain, S.N., 2012. Effect of thermal mass on performance of insulated building walls and the concept of energy savings potential. Appl. Energy 89, 430–442. https://doi.org/10.1016/j.apenergy.2011.08.009

American National Standards Institute, American Society of Heating, Refrigerating and Air-Conditioning Engineers, Illuminating Engineering Society of North America, 2007. ANSI/ASHRAE/IES Standard 90.1-2007 - Energy Standard for Buildings Except Low-Rise Residential Buildings, ANSI/ASHRAE/IES standard, 90.1-2007. American Society of Heating, Refrigerating and Air-Conditioning Engineers, Atlanta, GA.

American Society of Heating, Refrigerating and Air-Conditioning Engineers, 2013. 2013 ASHRAE Handbook: Fundamentals. ASHRAE, Atlanta, GA.

Arnault, A., Mathieu-Potvin, F., Gosselin, L., 2010. Internal surfaces including phase change materials for passive optimal shift of solar heat gain. Int. J. Therm. Sci. 49, 2148–2156. https://doi.org/10.1016/j.ijthermalsci.2010.06.021

Ascione, F., Bianco, N., De Masi, R., Mauro, G., Vanoli, G., 2015. Design of the Building Envelope: A Novel Multi-Objective Approach for the Optimization of Energy Performance and Thermal Comfort. Sustainability 7, 10809–10836. https://doi.org/10.3390/su70810809

Aste, N., Angelotti, A., Buzzetti, M., 2009. The influence of the external walls thermal inertia on the energy performance of well insulated buildings. Energy Build. 41, 1181–1187. https://doi.org/10.1016/j.enbuild.2009.06.005

Bastani, A., Haghighat, F., Kozinski, J., 2014. Designing building envelope with PCM wallboards: Design tool development. Renew. Sustain. Energy Rev. 31, 554–562. https://doi.org/10.1016/j.rser.2013.12.031

Chwieduk, D.A., 2016. Some aspects of energy efficient building envelope in high latitude countries. Sol. Energy 133, 194–206. https://doi.org/10.1016/j.solener.2016.03.068

CIBSE Guide A: Environmental design, 7th ed, 2006. . London.

Cole, R.J., 1999. Energy and greenhouse gas emissions associated with the construction of alternative structural systems. Build. Environ. 34, 335–348.

Czajkowski, Ł., Olek, W., Weres, J., Guzenda, R., 2016. Thermal properties of wood-based panels: specific heat determination. Wood Sci. Technol. 50, 537–545. https://doi.org/10.1007/s00226-016-0803-7

Di Perna, C., Stazi, F., Casalena, A.U., D'Orazio, M., 2011. Influence of the internal inertia of the building envelope on summertime comfort in buildings with high internal heat loads. Energy Build. 43, 200–206. https://doi.org/10.1016/j.enbuild.2010.09.007

ENQUÊTE SUR L'UTILISATION COMMERCIALE ET INSTITUTIONNELLE D'ÉNERGIE : BÂTIMENTS 2009 - M144-4-2-2013-fra.pdf, n.d.

Évolution de l'efficacité énergétique au Canada, de 1990 à 2009 [WWW Document], n.d. URL http://oee.nrcan.gc.ca/publications/statistiques/evolution11/index.cfm (accessed 8.11.16).

Fadzli Haniff, M., Selamat, H., Yusof, R., Buyamin, S., Sham Ismail, F., 2013. Review of HVAC scheduling techniques for buildings towards energy-efficient and cost-

effective operations. Renew. Sustain. Energy Rev. 27, 94–103. https://doi.org/10.1016/j.rser.2013.06.041
Gregory, K., Moghtaderi, B., Sugo, H., Page, A., 2008. Effect of thermal mass on the thermal performance of various Australian residential constructions systems. Energy Build. 40, 459–465. https://doi.org/10.1016/j.enbuild.2007.04.001
Grenfell Davies, M., 2004. Building Heat Transfer. Wiley, England.
Hacker, J.N., De Saulles, T.P., Minson, A.J., Holmes, M.J., 2008. Embodied and operational carbon dioxide emissions from housing: A case study on the effects of thermal mass and climate change. Energy Build. 40, 375–384. https://doi.org/10.1016/j.enbuild.2007.03.005
ISO 13786:2007, n.d. Thermal performance of building components - Dynamic thermal characteristics - Calculation methods.
Karlsson, J., Wadsö, L., Öberg, M., 2013. A conceptual model that simulates the influence of thermal inertia in building structures. Energy Build. 60, 146–151. https://doi.org/10.1016/j.enbuild.2013.01.017
Kossecka, E., Kosny, J., 2002. Influence of insulation configuration on heating and cooling loads in a continuously used building. Energy Build. 34, 321–331. https://doi.org/10.1016/S0378-7788(01)00121-9
Lo, C.-L., 2017. Environmental benefits of renewable building materials: A case study in Taiwan. Energy Build. 140, 236–244. https://doi.org/10.1016/j.enbuild.2017.02.010
Orosa, J.A., Oliveira, A.C., 2012. A field study on building inertia and its effects on indoor thermal environment. Renew. Energy 37, 89–96. https://doi.org/10.1016/j.renene.2011.06.009
Ramage, M.H., Burridge, H., Busse-Wicher, M., Fereday, G., Reynolds, T., Shah, D.U., Wu, G., Yu, L., Fleming, P., Densley-Tingley, D., Allwood, J., Dupree, P., Linden, P.F., Scherman, O., 2017. The wood from the trees: The use of timber in construction. Renew. Sustain. Energy Rev. 68, 333–359. https://doi.org/10.1016/j.rser.2016.09.107
Ramponi, R., Angelotti, A., Blocken, B., 2014. Energy saving potential of night ventilation: Sensitivity to pressure coefficients for different European climates. Appl. Energy 123, 185–195. https://doi.org/10.1016/j.apenergy.2014.02.041
Reynders, G., Nuytten, T., Saelens, D., 2013. Potential of structural thermal mass for demand-side management in dwellings. Build. Environ. 64, 187–199. https://doi.org/10.1016/j.buildenv.2013.03.010
Rijksen, D.O., Wisse, C.J., van Schijndel, A.W.M., 2010. Reducing peak requirements for cooling by using thermally activated building systems. Energy Build. 42, 298–304. https://doi.org/10.1016/j.enbuild.2009.09.007
Rossi, M., Rocco, V.M., 2014. External walls design: The role of periodic thermal transmittance and internal areal heat capacity. Energy Build. 68, 732–740. https://doi.org/10.1016/j.enbuild.2012.07.049
Sadineni, S.B., Madala, S., Boehm, R.F., 2011. Passive building energy savings: A review of building envelope components. Renew. Sustain. Energy Rev. 15, 3617–3631. https://doi.org/10.1016/j.rser.2011.07.014
Sansregret, S., Millette, J., 2009. Development of a functionality generating simulations of commercial and institutional buildings having representative charcteristics of a real

estate stock in Québec (Canada). Presented at the Eleventh International IBPSA Conference, Glasgow, Scotland.

Stazi, F., Vegliò, A., Di Perna, C., Munafò, P., 2013. Experimental comparison between 3 different traditional wall constructions and dynamic simulations to identify optimal thermal insulation strategies. Energy Build. 60, 429–441. https://doi.org/10.1016/j.enbuild.2013.01.032

Stevens, V., Kotol, M., Grunau, B., Craven, C., 2016. The Effect of Thermal Mass on Annual Heat Load and Thermal Comfort in Cold Climate Construction. J. Cold Reg. Eng. 30, 04015002. https://doi.org/10.1061/(ASCE)CR.1943-5495.0000092

Wang, L.-S., Ma, P., Hu, E., Giza-Sisson, D., Mueller, G., Guo, N., 2014. A study of building envelope and thermal mass requirements for achieving thermal autonomy in an office building. Energy Build. 78, 79–88. https://doi.org/10.1016/j.enbuild.2014.04.015

Ximenes, F.A., Grant, T., 2013. Quantifying the greenhouse benefits of the use of wood products in two popular house designs in Sydney, Australia. Int. J. Life Cycle Assess. 18, 891–908. https://doi.org/10.1007/s11367-012-0533-5

Yang, L., Li, Y., 2008. Cooling load reduction by using thermal mass and night ventilation. Energy Build. 40, 2052–2058. https://doi.org/10.1016/j.enbuild.2008.05.014

Zhu, L., Hurt, R., Correia, D., Boehm, R., 2009. Detailed energy saving performance analyses on thermal mass walls demonstrated in a zero energy house. Energy Build. 41, 303–310. https://doi.org/10.1016/j.enbuild.2008.10.003

**Figure captions**

**Figure 1:** Description of the different cases simulated in this paper

**Figure 2:** Heating, cooling (a), and total (b) energy intensities as a function of RSI value for the lightweight wall and three different thermal mass thicknesses (0.0254m, 0.254 m and 0.508 m) for concrete and wood walls

**Figure 3:** Heating, cooling (a), and total (b) energy intensities as a function of the thermal mass thickness ($L$) for RSI values: 4, 6, and 8

**Figure 4:** Discomfort indices due to higher and lower operative temperatures (a) and total discomfort index (b) as a function of the thermal mass thickness for RSI value 6

**Figure 5:** Hourly mean wall surface temperature for 4 cases on January 30th (a), March 18th (b), and June 29th (c)

**Figure 6:** Mean daily surface temperature swing vs thermal mass thickness ($L$) for RSI values: 4, 6, and 8

**Figure 7:** Internal areal heat capacity ($\kappa_1$) as a function of the thermal mass thickness ($L$) for RSI values: 4, 6, and 8

**Figure 8:** Heating, cooling (a), and total (b) energy intensities vs internal areal heat capacity ($\kappa_1$) for RSI values: 4, 6, and 8

**Figure 9:** Discomfort indices due to higher and lower operative temperatures (a) and total discomfort index (b) vs internal areal heat capacity ($\kappa_1$) for RSI values: 4, 6, and 8

**Figure 10:** Dynamic transmittance $|Y_{12}|$ vs thermal mass thickness for RSI value 6

**Figure 11:** Heating, cooling (a), and total (b) energy intensities vs dynamic transmittance $|Y_{12}|$ for RSI values: 4, 6, and 8

**Figure 12:** Discomfort indices due to higher and lower operative temperatures (a) and total discomfort index (b) vs dynamic transmittance $|Y_{12}|$ for RSI values: 4, 6, and 8

**Figure 13:** Decrement factor ($f$) vs dynamic transmittance $|Y_{12}|$ for RSI values: 4, 6, and 8

**Figure 14:** Time lag $\tau$ as a function of the thermal mass thickness ($L$) for RSI values: 4, 6, and 8

**Tables captions**

**Table 1:** Description of the wall assemblies considered in this study

**Table 2:** Description of the floor assembly considered in this study

**Table 3:** Thermal properties of the materials used in this study

**Table 4:** Schedule of the occupation rate

**Table 5:** Comparison of energy consumption between two test cases

**Table 6:** Symbols and color legend for Fig. 3−13, except Fig. 5

**Table 7:** Thermal properties of the different components of walls assemblies

**Table 8:** Comparison of the dynamic properties of envelopes obtained with the present numerical program and in Chapter 15.3 of (Grenfell Davies, 2004)

**Table 9:** Comparison of the dynamic properties of envelopes obtained with the present numerical program and by Rossi and Rocco (Rossi and Rocco, 2014)

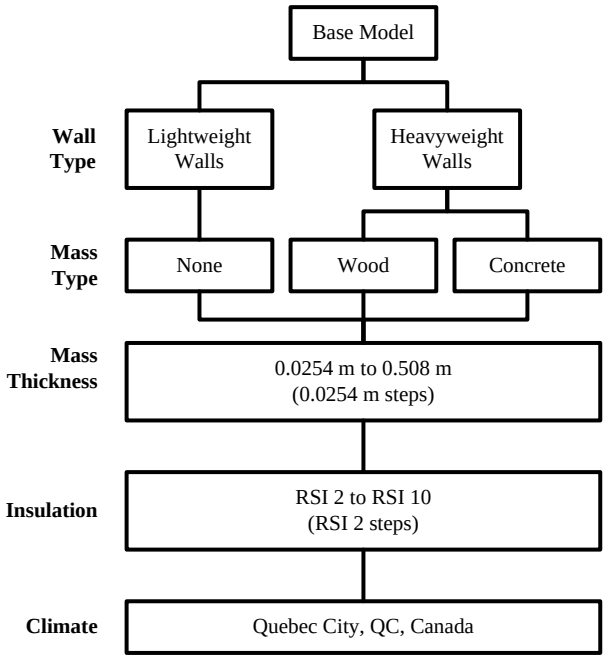
Base Model
Wall Type
Lightweight Walls
Heavyweight Walls
Mass Type
None
Wood
Concrete
Mass Thickness
0.0254 m to 0.508 m
(0.0254 m steps)
Insulation
RSI 2 to RSI 10
(RSI 2 steps)
Climate
Quebec City, QC, Canada

**Figure 1**

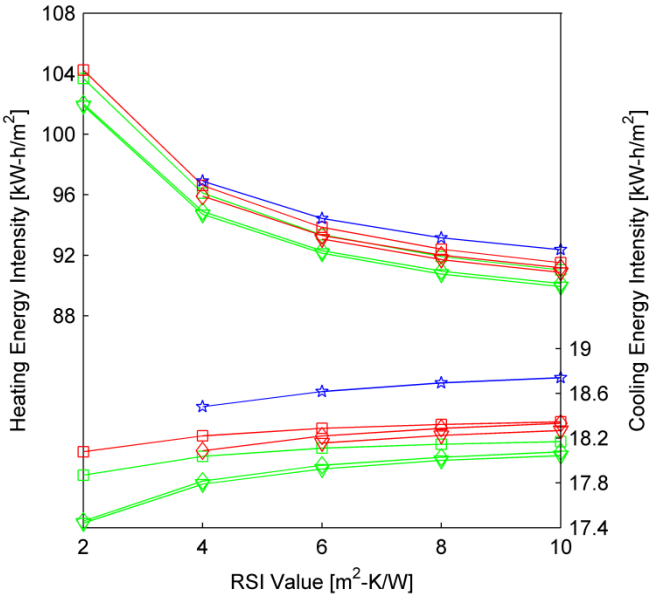
Heating Energy Intensity [kW-h/m2]
Cooling Energy Intensity [kW-h/m2]
RSI Value [m2-K/W]
108
104
100
96
92
88
19
18.6
18.2
17.8
17.4
2
4
6
8
10

a)

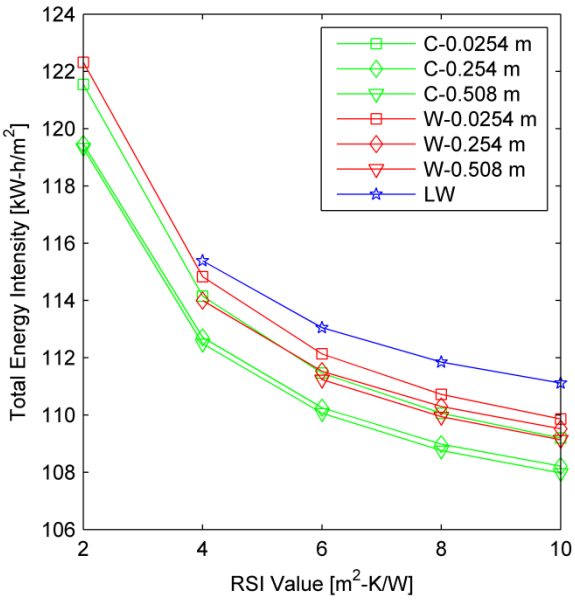
Total Energy Intensity [kW-h/m2]
RSI Value [m2-K/W]
C-0.0254 m
C-0.254 m
C-0.508 m
W-0.0254 m
W-0.254 m
W-0.508 m
LW
124
122
120
118
116
114
112
110
108
106
2
4
6
8
10

b)

**Figure 2**

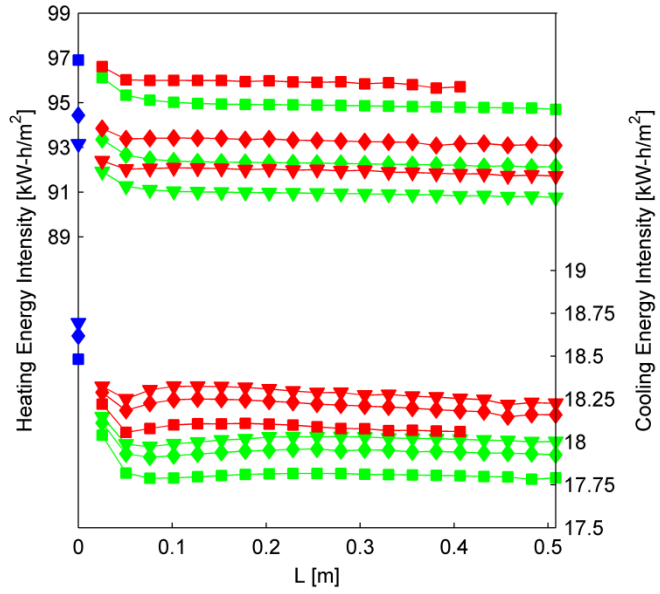
Heating Energy Intensity [kW-h/m2]
Cooling Energy Intensity [kW-h/m2]
L [m]
99
97
95
93
91
89
19
18.75
18.5
18.25
18
17.75
17.5
0
0.1
0.2
0.3
0.4
0.5

a)

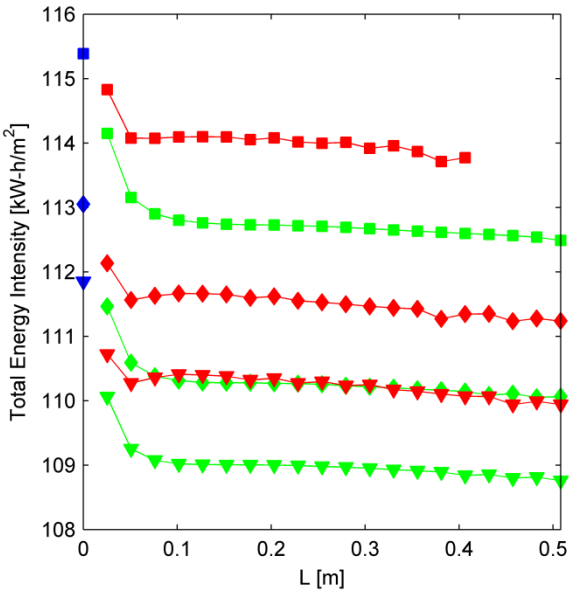
Total Energy Intensity [kW-h/m2]
L [m]
116
115
114
113
112
111
110
109
108
0
0.1
0.2
0.3
0.4
0.5

b)

**Figure 3**

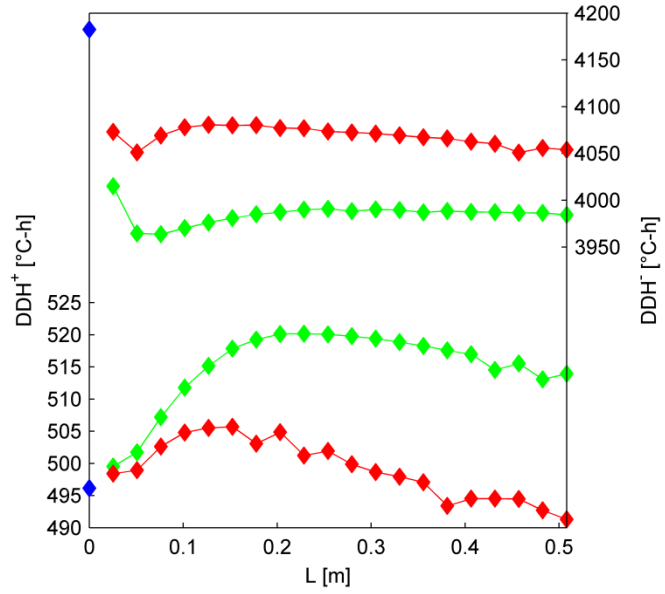
DDH+ [°C-h]
DDH- [°C-h]
L [m]
525
520
515
510
505
500
495
490
4200
4150
4100
4050
4000
3950
0
0.1
0.2
0.3
0.4
0.5

a)

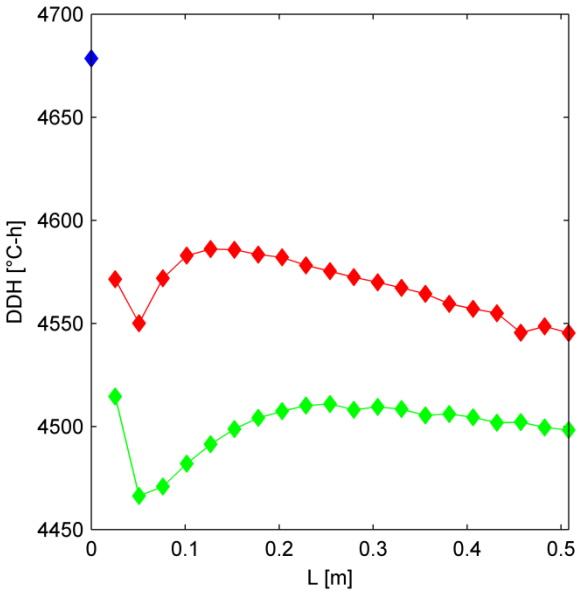
DDH [°C-h]
L [m]
4700
4650
4600
4550
4500
4450
0
0.1
0.2
0.3
0.4
0.5

b)

**Figure 4**

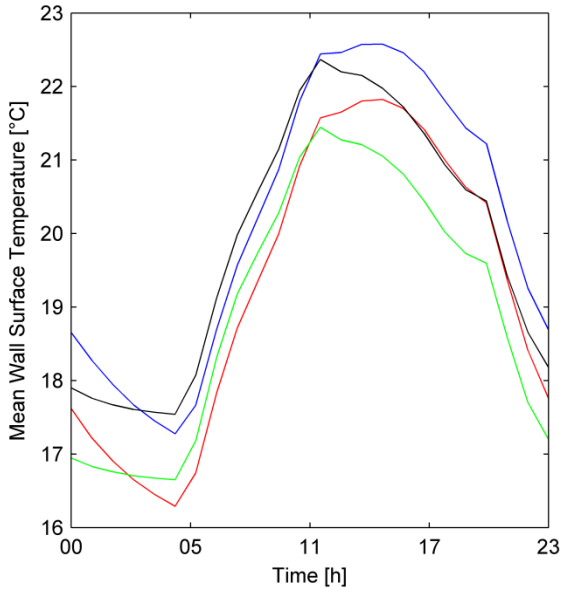
Mean Wall Surface Temperature [°C]
23
22
21
20
19
18
17
16
00
05
11
17
23
Time [h]

a)

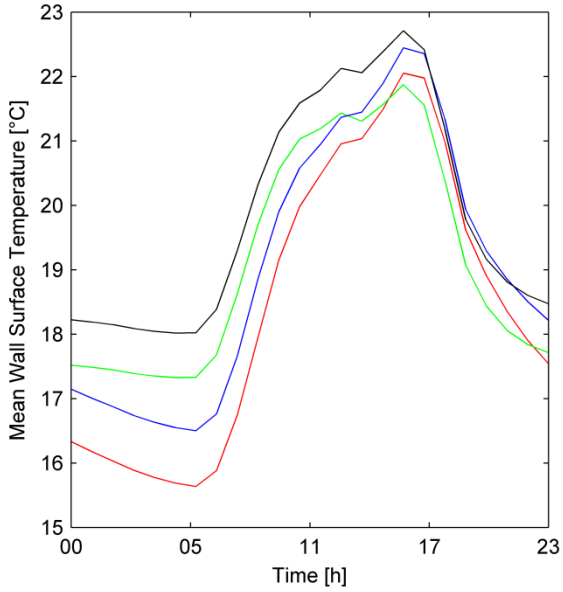
Mean Wall Surface Temperature [°C]
23
22
21
20
19
18
17
16
15
00
05
11
17
23
Time [h]

b)

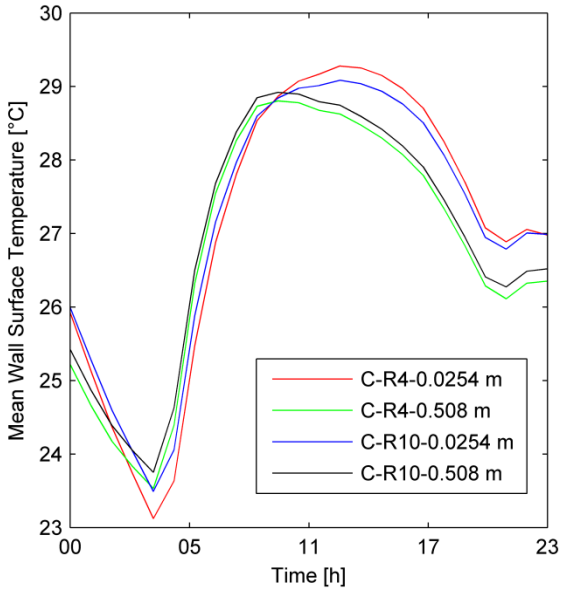
Mean Wall Surface Temperature [°C]
Time [h]
30
29
28
27
26
25
24
23
00
05
11
17
23
C-R4-0.0254 m
C-R4-0.508 m
C-R10-0.0254 m
C-R10-0.508 m

c)

**Figure 5**

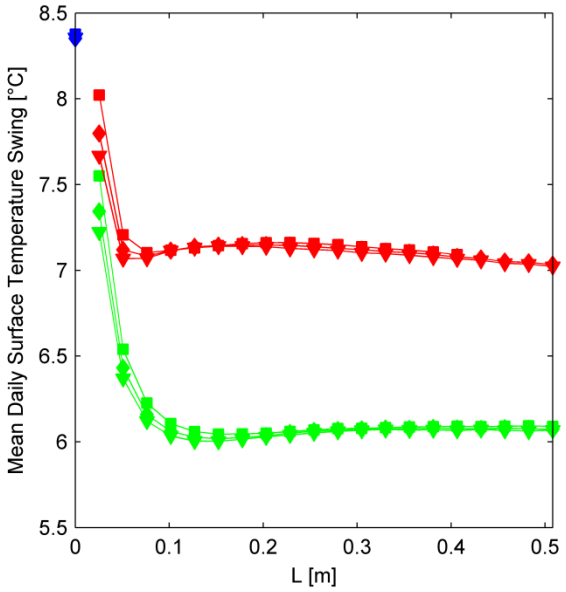
Mean Daily Surface Temperature Swing [°C]
8.5
8
7.5
7
6.5
6
5.5
0
0.1
0.2
0.3
0.4
0.5
L [m]

**Figure 6**

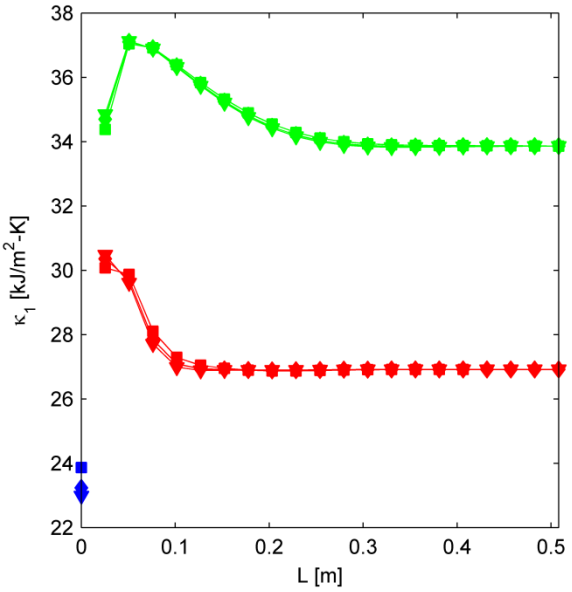


**Figure 7**

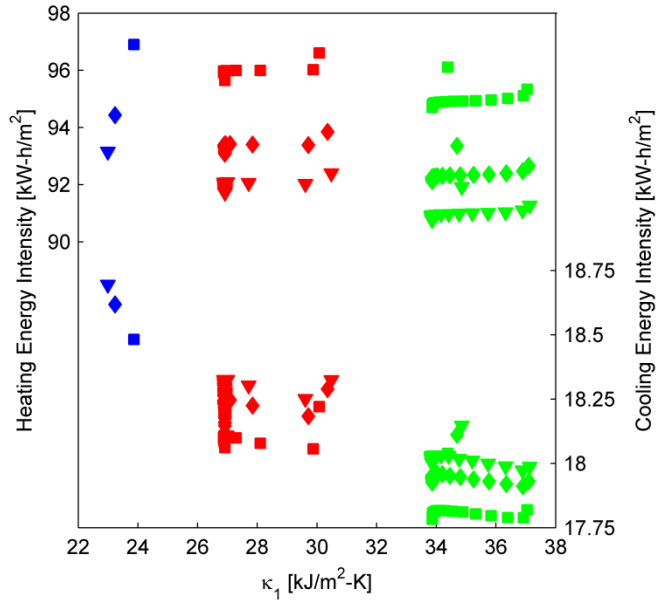
Heating Energy Intensity [kW-h/m$^2$]
Cooling Energy Intensity [kW-h/m$^2$]
$\kappa_1$ [kJ/m$^2$-K]
98
96
94
92
90
18.75
18.5
18.25
18
17.75
22
24
26
28
30
32
34
36
38

a)

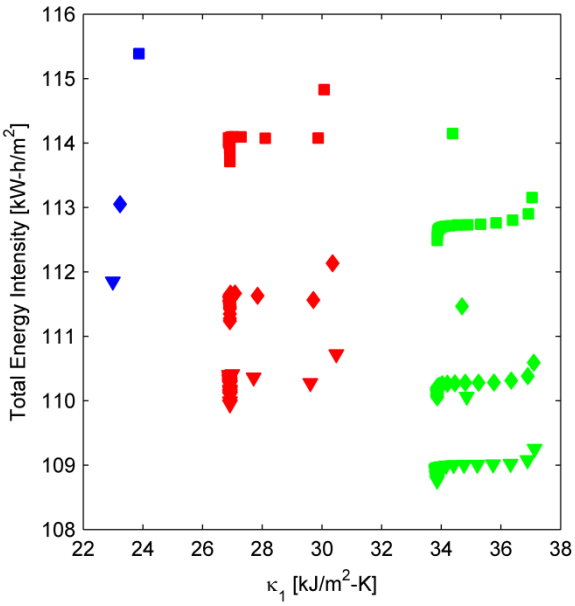
Total Energy Intensity [kW-h/m$^2$]
$\kappa_1$ [kJ/m$^2$-K]
116
115
114
113
112
111
110
109
108
22
24
26
28
30
32
34
36
38

b)

**Figure 8**

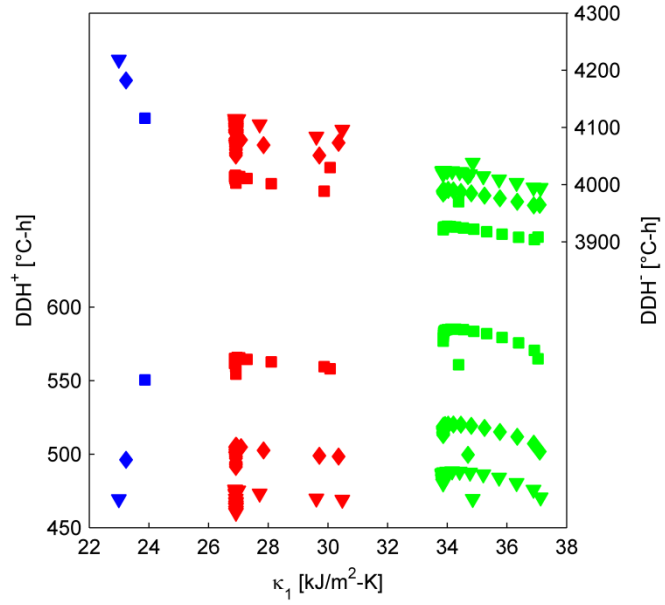
4300
4200
4100
4000
3900
DDH- [°C-h]
DDH+ [°C-h]
600
550
500
450
22
24
26
28
30
32
34
36
38
κ1 [kJ/m2-K]

a)

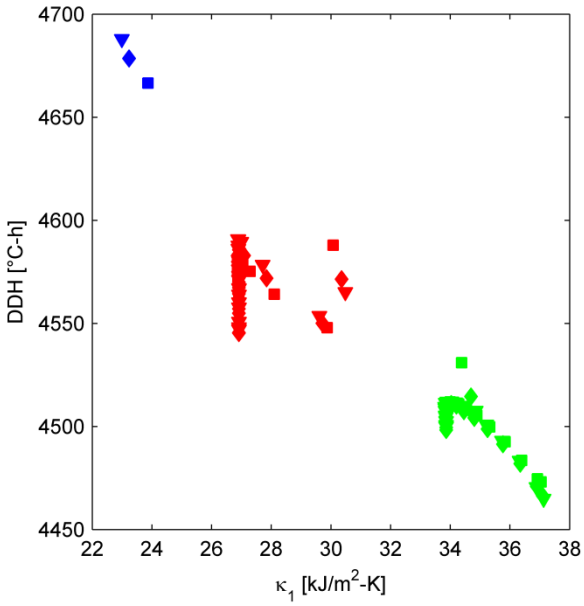
4700
4650
4600
4550
4500
4450
DDH [°C-h]
22
24
26
28
30
32
34
36
38
κ1 [kJ/m2-K]

b)

**Figure 9**

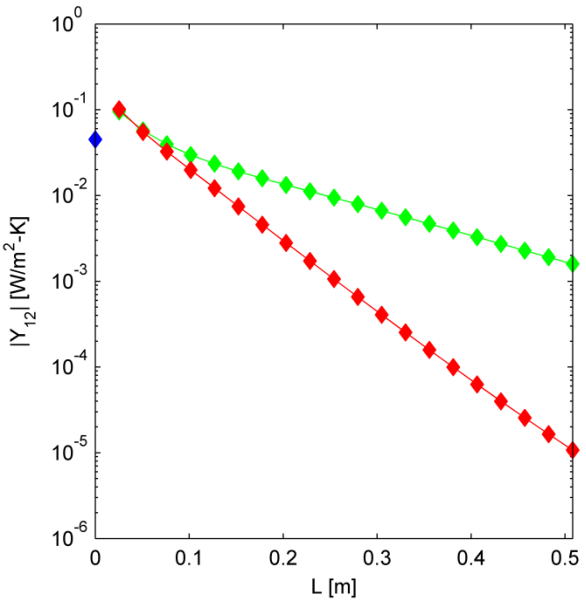


**Figure 10**

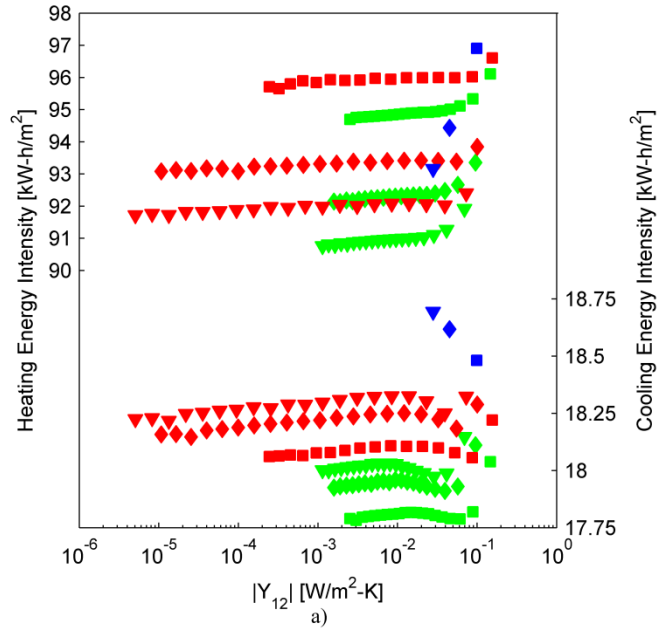
Heating Energy Intensity [kW-h/m2]
Cooling Energy Intensity [kW-h/m2]
|Y12| [W/m2-K]
a)

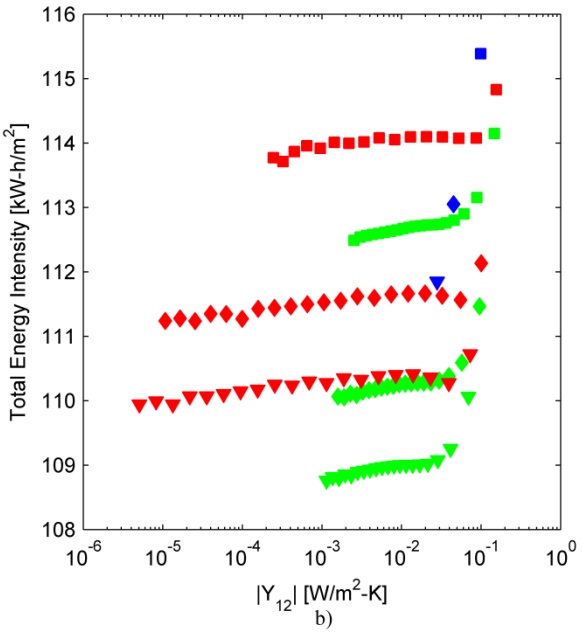
Total Energy Intensity [kW-h/m2]
|Y12| [W/m2-K]
b)

**Figure 11**

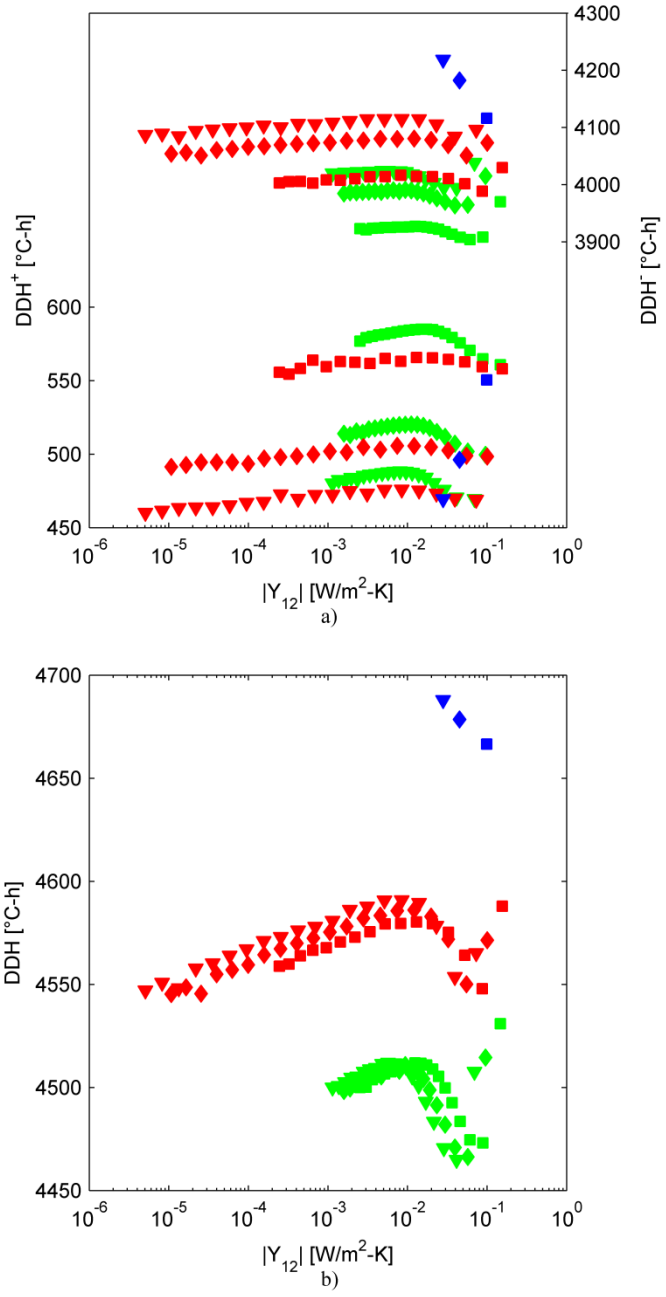
4300
4200
4100
4000
3900
DDH+ [°C-h]
DDH- [°C-h]
600
550
500
450
10-6
10-5
10-4
10-3
10-2
10-1
100
|Y12| [W/m2-K]
a)
4700
4650
4600
4550
4500
4450
DDH [°C-h]
|Y12| [W/m2-K]
b)

**Figure 12**

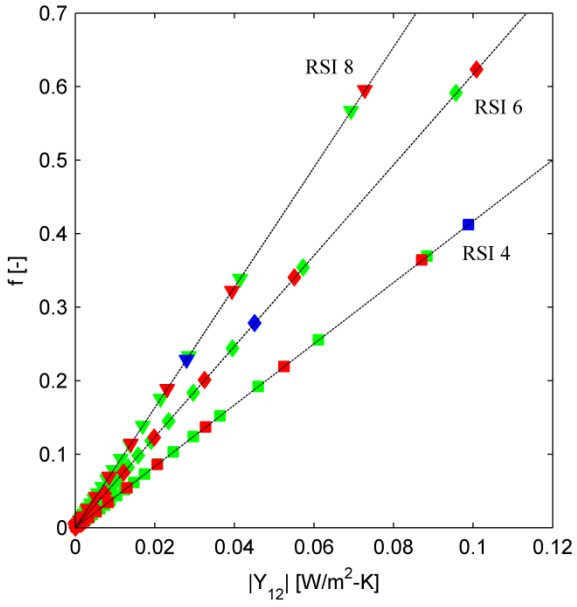
RSI 8
RSI 6
RSI 4
f [-]
|Y12| [W/m2-K]
0
0.1
0.2
0.3
0.4
0.5
0.6
0.7
0.02
0.04
0.06
0.08
0.1
0.12

**Figure 13**

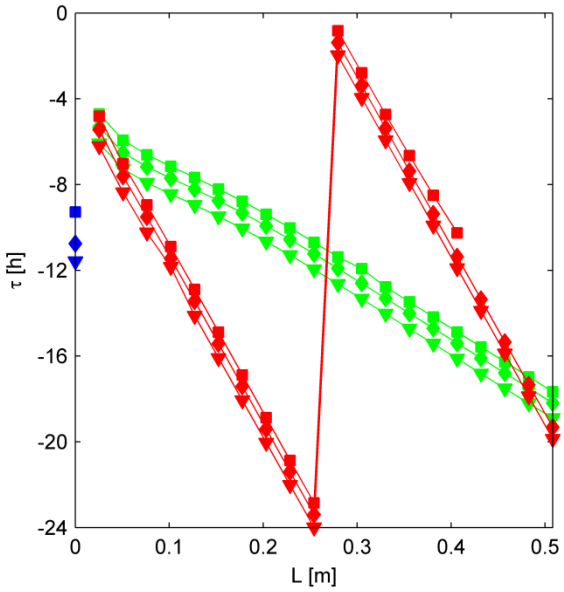


**Figure 14**

**Table 1**

| | CLT Construction | Heavyweight concrete construction | Lightweight construction |
|---|---|---|---|
| Exterior | Wood siding (0.015875 m) | Wood siding (0.015875 m) | Wood siding (0.015875 m) |
| Layer 1 | Air layer (0.0254 m) | Air layer (0.0254 m) | Air layer (0.0254 m) |
| Layer 2 | Polyisocyanurate* | Polyisocyanurate* | Polyisocyanurate* |
| Layer 3 | CLT panel* | Concrete layer* | Wood fiber panel (0.0127 m) |
| Layer 4 | Air layer (0.01905 m) | Air layer (0.01905 m) | Wood studs \| Rock wool |
| Layer 5 | Gypsum (0.015875 m) | Gypsum (0.015875 m) | OSB (0.0127 m) |
| Layer 6 | - | - | Wood studs \| Air |
| Layer 7 | - | - | Gypsum (0.015875 m) |

*Layers for which the thickness is modified in the simulations.

**Table 2**

| | Floor construction |
|---|---|
| Floor above | Carpet (0.00635 m) |
| Layer 1 | Acoustic tile (0.01905 m) |
| Layer 2 | Air layer (0.1778 m) |
| Layer 3 | Rock wool (0.1016 m) |
| Ceiling below | Gypsum (0.03175 m) |

**Table 3**

| | $k$ [W/m-K] | $\rho$ [kg/m$^3$] | $c_p$ [J/kg-K] | $R''$ [m$^2$-K/W] |
|---|---|---|---|---|
| Acoustic tile | 0.0600 | 368.42 | 585.76 | - |
| Air layers | - | - | - | 0.1500 |
| Carpet | 0.0600 | 288.00 | 1380.00 | - |
| CLT panel | 0.1211 | 2510.40 | 592.68 | - |
| Concrete layer | 1.3110 | 2242.60 | 836.80 | - |
| Gypsum | 0.1601 | 800.92 | 836.80 | - |
| OSB | 0.1060 | 650.00 | 1880.00 | - |
| Polyisocyanurate | 0.0202 | 32.04 | 920.48 | - |
| Wood studs \| Rock wool | 0.0270 | 66.97 | 821.80 | - |
| Wood siding | 0.1000 | 530.00 | 1880.00 | - |
| Wood studs \| Air | - | - | - | 0.1602 |
| Wood fiber panel | 0.0600 | 1090.00 | 1000.00 | - |
| Rock wool | 0.0201 | 32.04 | 709.61 | - |

**Table 4**

| Monday – Friday | | Saturday | | Sunday and Holidays | |
|---|---|---|---|---|---|
| 6:00 – 7:00 | 0.10 | 6:00 – 8:00 | 0.10 | 6:00 – 18:00 | 0.05 |
| 7:00 – 8:00 | 0.20 | 8:00 – 12:00 | 0.30 | 18:00 – 24:00 | 0.00 |
| 8:00 – 12:00 | 0.95 | 12:00 – 17:00 | 0.10 | 24:00 – 6:00 | 0.00 |
| 12:00 – 13:00 | 0.50 | 17:00 – 19:00 | 0.05 | | |
| 13:00 – 17:00 | 0.95 | 19:00 – 22:00 | 0.00 | | |
| 17:00 – 18:00 | 0.30 | 22:00 – 6:00 | 0.00 | | |
| 18:00 – 22:00 | 0.10 | | | | |
| 22:00 – 24:00 | 0.05 | | | | |
| 24:00 – 6:00 | 0.00 | | | | |

**Table 5**

| | Archetype | Present model |
|---|---|---|
| Energy consumption, heating [kW-h/m$^2$] | 88.7 | 86.8 |
| Energy consumption, cooling [kW-h/m$^2$] | 28.0 | 16.5 |
| Total [kW-h/m$^2$] | 116.7 | 103.3 |
| Ratio heating/cooling | 0.76 | 0.84 |

**Table 6**

| | Concrete | Wood | Lightweight |
|---|---|---|---|
| RSI 4 | ■ | ■ | ■ |
| RSI 6 | ◆ | ◆ | ◆ |
| RSI 8 | ▼ | ▼ | ▼ |

**Table 7**

| | $l$ [m] | $k$ [W/m-K] | $\rho$ [kg/m$^3$] | $c_p$ [J/kg-K] |
|---|---|---|---|---|
| ***Building Heat Transfer wall*** (Grenfell Davies, 2004) | | | | |
| Plaster | 0.013 | 0.500 | 1300 | 1000 |
| Concrete | 0.200 | 0.190 | 600 | 1000 |
| ***Improved External walls*** (Rossi and Rocco, 2014) | | | | |
| ***L02_k1*** | | | | |
| Mineralized wooden board | 0.025 | 0.260 | 1250 | 2100 |
| CLT timber panel | 0.100 | 0.130 | 500 | 1600 |
| Vacuum insulation panels | 0.050 | 0.010 | 200 | 1050 |
| Plywood panel | 0.010 | 0.130 | 450 | 1600 |
| ***L03_k1*** | | | | |
| Mineralized wooden board | 0.030 | 0.260 | 1250 | 2100 |
| Sheep wool insulation | 0.040 | 0.040 | 30 | 1000 |
| CLT timber panel | 0.100 | 0.130 | 500 | 1600 |
| Wood-fiber insulation board | 0.070 | 0.055 | 200 | 2500 |
| Lime or lime and cement plaster | 0.030 | 1.000 | 2000 | 1130 |
| ***L04_k1*** | | | | |
| Mineralized wooden board | 0.030 | 0.260 | 1250 | 2100 |

| | | | | |
|---|---|---|---|---|
| Sheep wool insulation | 0.040 | 0.040 | 30 | 1000 |
| Vapor diffusion retarder | 0.000 | 0.220 | 238 | 1700 |
| OSB | 0.018 | 0.130 | 650 | 1700 |
| Cellulose insulation | 0.140 | 0.040 | 60 | 1900 |
| Wooden board | 0.025 | 0.130 | 450 | 2700 |
| Wood-fiber insulation board | 0.015 | 0.055 | 200 | 2500 |
| Lime or lime and cement plaster | 0.015 | 1.000 | 2000 | 1130 |

**Table 8**

| | Wall thickness [m] | $U$ [W/m$^2$-K] | $f$ [-] | $\tau$ [h] | $\lvert Y_{12} \rvert$ [W/m$^2$-K] | $\kappa_1$ [kJ/m$^2$-K] |
|---|---|---|---|---|---|---|
| Ref. (Grenfell Davies, 2004) | 0.213 | 0.79 | 0.550 | -6.90 | 0.44 | - |
| Present model | 0.213 | 0.79 | 0.559 | -6.76 | 0.44 | 35.9 |

**Table 9**

| | Wall thickness [m] | $U$ [W/m$^2$-K] | $f$ [-] | $\tau$ [h] | $\lvert Y_{12} \rvert$ [W/m$^2$-K] | $\kappa_1$ [kJ/m$^2$-K] |
|---|---|---|---|---|---|---|
| **L02_k1** | | | | | | |
| Ref. (Rossi and Rocco, 2014) | 0.185 | 0.16 | 0.235 | 11.39 | 0.04 | 53.4 |
| Present model | 0.185 | 0.16 | 0.241 | 12.64 | 0.04 | 55.1 |
| **L03_k1** | | | | | | |
| Ref. (Rossi and Rocco, 2014) | 0.270 | 0.30 | 0.122 | 14.30 | 0.04 | 53.5 |
| Present model | 0.270 | 0.30 | 0.120 | 14.55 | 0.04 | 55.0 |
| **L04_k1** | | | | | | |
| Ref. (Rossi and Rocco, 2014) | 0.283 | 0.19 | 0.219 | 13.34 | 0.04 | 54.5 |
| Present model | 0.283 | 0.18 | 0.217 | 13.49 | 0.04 | 56.1 |